^{68}Ga/^{177}Lu-NeoBOMB1, a Novel Radiolabeled GRPR Antagonist for Theranostic Use in Oncology

Simone U. Dalm*[1], Ingrid L. Bakker*[1], Erik de Blois[1], Gabriela N. Doeswijk[1], Mark W. Konijnenberg[1], Francesca Orlandi[2], Donato Barbato[2], Mattia Tedesco[2], Theodosia Maina[3], Berthold A. Nock[3], and Marion de Jong[1]

[1]*Department of Radiology and Nuclear Medicine, Erasmus MC, Rotterdam, The Netherlands;* [2]*Advanced Accelerator Applications, Colleretto Giacosa, Italy; and* [3]*Molecular Radiopharmacy, INRASTES, NCSR "Demokritos", Athens, Greece*

Because overexpression of the gastrin-releasing peptide receptor (GRPR) has been reported on various cancer types, for example, prostate cancer and breast cancer, targeting this receptor with radioligands might have a significant impact on staging and treatment of GRPR-expressing tumors. NeoBOMB1 is a novel DOTA-coupled GRPR antagonist with high affinity for GRPR and excellent in vivo stability. The purpose of this preclinical study was to further explore the use of NeoBOMB1 for theranostic application by determining the biodistribution of ^{68}Ga-NeoBOMB1 and ^{177}Lu-NeoBOMB1. **Methods:** PC-3 tumor–xenografted BALB/c *nu/nu* mice were injected with either approximately 13 MBq/250 pmol ^{68}Ga-NeoBOMB1 or a low (~1 MBq/200 pmol) versus high (~1 MBq/10 pmol) peptide amount of ^{177}Lu-NeoBOMB1, after which biodistribution and imaging studies were performed. At 6 time points (15, 30, 60, 120, 240, and 360 min for ^{68}Ga-NeoBOMB1 and 1, 4, 24, 48, 96, and 168 h for ^{177}Lu-NeoBOMB1) postinjection tumor and organ uptake was determined. To assess receptor specificity, additional groups of animals were coinjected with an excess of unlabeled NeoBOMB1. Results of the biodistribution studies were used to determine pharmacokinetics and dosimetry. Furthermore, PET/CT and SPECT/MRI were performed. **Results:** Injection of approximately 250 pmol ^{68}Ga-NeoBOMB1 resulted in a tumor and pancreas uptake of 12.4 ± 2.3 and 22.7 ± 3.3 percentage injected dose per gram (%ID/g) of tissue, respectively, at 120 min after injection. ^{177}Lu-NeoBOMB1 biodistribution studies revealed a higher tumor uptake (17.9 ± 3.3 vs. 11.6 ± 1.3 %ID/g of tissue at 240 min after injection) and a lower pancreatic uptake (19.8 ± 6.9 vs. 105 ± 13 %ID/g of tissue at 240 min after injection) with the higher peptide amount injected, leading to a significant increase in the absorbed dose to the tumor versus the pancreas (200 pmol, 570 vs. 265 mGy/MBq; 10 pmol, 435 vs. 1393 mGy/MBq). Using these data to predict patient dosimetry, we found a kidney, pancreas, and liver exposure of 0.10, 0.65, and 0.06 mGy/MBq, respectively. Imaging studies resulted in good visualization of the tumor with both ^{68}Ga-NeoBOMB1 and ^{177}Lu-NeoBOMB1. **Conclusion:** Our findings indicate that ^{68}Ga- or ^{177}Lu-labeled NeoBOMB1 is a promising radiotracer with excellent tumor uptake and favorable pharmacokinetics for imaging and therapy of GRPR-expressing tumors.

Key Words: cancer theranostics; gastrin releasing peptide receptor; GRPR antagonist; biodistribution; dosimetry

J Nucl Med 2017; 58:293–299
DOI: 10.2967/jnumed.116.176636

The gastrin-releasing peptide receptor (GRPR), also known as bombesin receptor subtype 2, is a G-protein–coupled receptor expressed in various organs, including those of the gastrointestinal tract and the pancreas (*1,2*). On binding of a suitable ligand, the GRPR is activated, eliciting multiple physiologic processes, such as regulation of exocrine and endocrine secretion (*1,2*). In the past decades, GRPR expression has been reported in various cancer types, including prostate cancer and breast cancer (*3,4*). Therefore, the GRPR became an interesting target for receptor-mediated tumor imaging and treatment, such as peptide receptor scintigraphy and peptide receptor radionuclide therapy (*2*). After the successful use of radiolabeled somatostatin peptide analogs in neuroendocrine tumors for nuclear imaging and therapy (*5,6*), multiple radiolabeled GRPR radioligands have been synthesized and studied in preclinical as well as in clinical studies, mostly in prostate cancer patients. Examples of such peptide analogs include AMBA, the Demobesin series, and MP2653 (*7–11*). Recent studies have shown a preference for GRPR antagonists compared with GRPR agonists (*12,13*). Compared with receptor agonists, antagonists often show higher binding and favorable pharmacokinetics (*14*). Also, clinical studies with radiolabeled GRPR agonists reported unwanted side effects in patients caused by activation of the GRPR after binding of the peptide to the receptor (*15*).

Although imaging and treatment with radiolabeled GRPR peptide analogs is not yet approved for routine clinical practice, progress made over the years led to new diagnostic radiotracers, which are most promising. On the route to developing a new successful imaging and treatment strategy for GRPR-expressing tumors, the development of radiotracers with favorable pharmacokinetics that can be labeled with different radionuclides is an essential step. Further studies are now needed to optimize the use of GRPR radioligands for imaging and treatment of GRPR-expressing tumors to determine the clinical value of GRPR-targeting radiotracers.

In this study, we explored the use of a novel DOTA-coupled GRPR antagonist, NeoBOMB1, derived from a previously reported

Received May 25, 2016; revision accepted Aug. 17, 2016.
For correspondence or reprints contact: Simone Dalm, Rm. 2510, P.O. Box 2040, 3000 CA Rotterdam, The Netherlands.
E-mail: s.dalm@erasmusmc.nl
*Contributed equally to this work.
Published online Sep. 8, 2016.

GRPR antagonist, SB3 (*16*). The peptidic part of NeoBOMB1, however, is based on a different GRPR antagonist first described by Heimbrook et al. (*17*) and generated by modification of the C-terminal Leu^{13}-Met^{14}-NH_2 and the replacement of Asn^6 by $DPhe^6$ of native bombesin(6-14). NeoBOMB1 was chosen for further studies because of its improved affinity for the GRPR (*18,19*). Coupling of the antagonist to a DOTA chelator enables labeling with different radionuclides such as ^{68}Ga (for PET), ^{111}In (for SPECT), and ^{177}Lu (for radionuclide therapy), which makes theranostic use of NeoBOMB1 possible. In a preliminary communication on NeoBOMB1, a GRPR affinity in the low nanomolar range for ^{nat}Ga-NeoBOMB1 and excellent in vivo stability of ^{67}Ga-NeoBOMB1 were reported (*18*).

The aim of our study was to further explore the perspectives of ^{68}Ga-NeoBOMB1 and ^{177}Lu-NeoBOMB1 for clinical translation by performing biodistribution studies in PC-3–xenografted mice. Two peptide amounts of ^{177}Lu-NeoBOMB1 were studied to define the optimal peptide amount for increasing tumor targeting while minimizing background radioactivity levels. Data of the ^{177}Lu-NeoBOMB1 biodistribution studies were used to determine dosimetry in mice and to predict dosimetry in humans.

MATERIALS AND METHODS

Radiotracer and Radiolabeling Procedure

NeoBOMB1 (Advanced Accelerator Applications) (Fig. 1) (*20*) was diluted in ultra-pure water, and concentration and chemical purity were monitored with an in-house–developed titration method (*21*). Labeling of NeoBOMB1 was based on a previously published kit approach by Castaldi et al. (*22*). Radioactivity was added (60 MBq/nmol ^{68}Ga or 100 MBq/nmol ^{177}Lu) to a vial containing all the necessary excipients, for example, buffer, antioxidants, and peptide; subsequently, this vial was heated at 85°C for 7 or 20 min, respectively. To measure radiometal incorporation, quality control was performed by instant thin-layer chromatography on silica gel using 0.1 M citrate (pH 5) or 1 M ammonium acetate/methanol (30/70 v/v) as buffers. High-performance liquid chromatography was performed with a gradient of methanol and 0.1% trifluoroacetic acid to determine radiochemical purity. Both ^{68}Ga-NeoBOMB1 and ^{177}Lu-NeoBOMB1 were diluted in phosphate-buffered saline plus a tensioactive agent to prevent sticking of the peptide, before injection in animals.

Animal Model

All animal studies were conducted in agreement with the Animal Welfare Committee requirements of Erasmus MC and in accordance with accepted guidelines. Male BALB/c *nu/nu* animals (6–8 wk) (Janvier) were subcutaneously (right shoulder) injected with 150 μL of inoculation medium (1/3 Matrigel high concentration [Corning] and 2/3 Hank's balanced salt solution [Thermofisher Scientific]) containing 5×10^6 cells of the GRPR-expressing human-derived prostate cancer cell line PC-3 (American Type Culture Collection). In vivo imaging and biodistribution studies were performed 3–4 wk after tumor cell inoculation, when tumor size was 340 ± 114 mm^3.

Imaging Studies

Mice (n = 2 per radiotracer) were injected with 50 μL of approximately 11.5 MBq/230 pmol ^{68}Ga-NeoBOMB1 or 200 μL of 20 MBq/200 pmol ^{177}Lu-NeoBOMB1, after which PET/CT or SPECT/MRI was performed.

The PET/CT scans were obtained at 60 min after injection of ^{68}Ga-NeoBOMB1 in a small-animal SPECT/PET/CT scanner (VECTor/CT; Milabs) under isoflurane/O_2 anesthesia. Whole-body scans were acquired for 120 min (48 projections, 38 s/projection) using a special collimator with clustered pinholes for high-energy photons. The collimator contains 162 pinholes with a diameter of 0.7 mm grouped in clusters of 4. Reconstruction was performed using a pixel-based ordered-subset expectation maximization method (4 subsets, 30 iterations) and visualized with Vivoquant (InVicro). A postreconstruction 3-dimensional gaussian filter was applied (1.2 mm full width at half maximum).

Whole-body SPECT images were obtained 240 min after injection of ^{177}Lu-NeoBOMB1 under isoflurane/O_2 anesthesia, using a 4-head multipinhole system (NanoScan SPECT/MRI; Mediso Medical Imaging). The images were acquired using 28 projections (40 s/projection) and reconstructed using the ordered-subset expectation maximization method and a voxel size of 0.25 × 0.25 × 0.25 mm and a scan time of 47 min. Coronal T2-weighted images were acquired with a 2-dimensional fast spin echo sequence on a 1-T permanent magnet (Mediso) with a 35-mm transmit/receive solenoid coil. Scan parameters used were echo time/repetition time, 4,500/39 ms; number of signals averaged, 4; field of view, 70 mm; resolution, 0.4 × 0.4 × 0.8 mm, with 0.1-mm spacing between slices and a scan time of 10 min.

Biodistribution Studies

Biodistribution studies were performed to determine tumor and organ uptake of ^{68}Ga-NeoBOMB1. Animals (n = 4 for each time point) were injected intravenously with an average of 13 MBq/250 pmol ^{68}Ga-NeoBOMB1 (injected volume, 50 μL) at t = 0. At 6 selected time points (15, 30, 60, 120, 240, and 360 min) after injection, animals were euthanized and organs and tumors were excised and their radioactivity uptake was determined. For the ^{177}Lu-NeoBOMB1 biodistribution studies, animals were injected with either 1 MBq/200 pmol or 1 MBq/10 pmol ^{177}Lu-NeoBOMB1 (injected volume, 200 μL) to determine the peptide amount with optimal tumor-to-background ratio. Four, 24, 48, 96, and 168 h after injection, animals were euthanized, organs were collected, and radiotracer uptake was determined (n = 4 for each concentration per time point). For both the ^{68}Ga-NeoBOMB1 and the ^{177}Lu-NeoBOMB1 biodistribution studies, the following organs were collected: blood, lungs, spleen, pancreas, kidneys, liver, organs of the gastrointestinal tract (stomach, intestine, caecum, and colon), muscle, tail, and tumor. To confirm receptor specificity of radiotracer uptake, PC-3–xenografted mice were coinjected with either ^{68}Ga-NeoBOMB1 or ^{177}Lu-NeoBOMB1 plus an excess (40 nmol) of unlabeled NeoBOMB1 (n = 2 and 4, respectively), after which tumor and organ uptake was determined 120 and 240 min after injection, respectively.

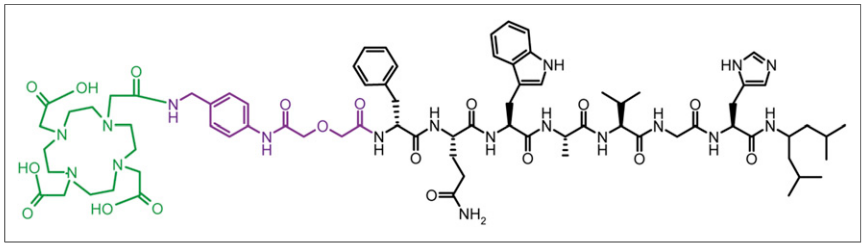

FIGURE 1. Chemical structure of NeoBOMB1. Green = DOTA chelator; purple = spacer; black = binding domain.

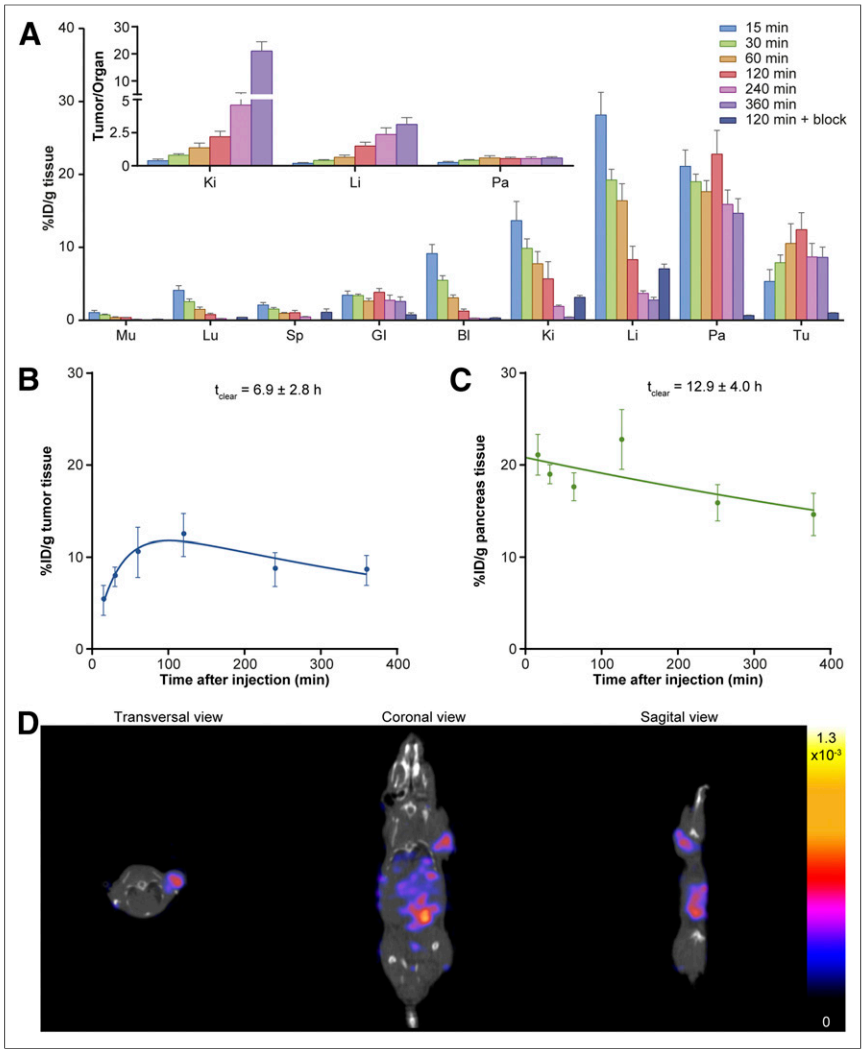

FIGURE 2. ^{68}Ga-NeoBOMB1 biodistribution and imaging. (A) Biodistribution of approximately 13 MBq/250 pmol ^{68}Ga-NeoBOMB1. Tumor-to-organ ratios are displayed in upper bar graph. (B and C) Pharmacokinetic modeling of ^{68}Ga-NeoBOMB1 tumor and pancreas uptake, respectively. (D) PET/CT images acquired 60 min after injection of 11.5 MBq/230 pmol ^{68}Ga-NeoBOMB1. Tumor is located on the shoulder. Bl = blood; Gl = gastrointestinal tract; Ki = kidney; Li = liver; Lu = lungs; Mu = muscle; Pa = pancreas; Sp = spleen; Tu = PC-3 tumor.

After tumor and organs were collected, the samples were weighed and counted in a γ-counter (1480 WIZARD automatic γ-counter; PerkinElmer) to determine the percentage injected dose per gram of tissue (%ID/g of tissue). For γ-counter measurements, an isotope specific energy window, a counting time of 60 s, and a counting error of 5% or less were used.

The radioactivity uptake in tumor and organs was corrected for the percentage of radioactivity measured in the tail.

Dosimetry

Kinetic analysis of the biodistribution data was performed to determine uptake and clearance characteristics of the radiotracers. For ^{177}Lu-NeoBOMB1, the resulting time–activity concentration curves through the uptake data were used to calculate the absorbed doses to the organs and tumor. The mouse dosimetry was performed using the RAdiation Dose Assessment Resource realistic mouse model (*23*). The absorbed dose to an organ, D_{organ}, was calculated according to the MIRD scheme (*24*): $D_{organ} = m_{organ} \times \sum_{src} TIAC_{src} \times S(organ \leftarrow src)$, with $TIAC_{src}$ the time-integrated activity concentration $TIAC_{src} = \int_0^\infty \frac{\%IA_{src}}{g}(t)dt$ and $S(organ \leftarrow src)$ the absorbed dose rate per unit activity in the source, src, for all source and organ combinations. The organ mass, m_{organ}, is taken from a reference mouse phantom of 25 g to obtain invariance to the measured organ weights. Tumor dosimetry was performed in the same way with the S values from Stabin and Konijnenberg (*25*).

Extrapolation of the mouse biodistribution data to estimate human dosimetry was performed according to the methods of Stabin (*26*). Only organ uptake values were extrapolated, and time-scaling was not applied. Two methods were applied for translation of the mice time-integrated activity concentration to human time-integrated activity concentration for each organ:

$$TIAC_{human} = TIAC_{mouse} \times \frac{M_{mouse}}{M_{human}},$$

by the ratio in body weights: M_{mouse} = 25 g and M_{human} = 70 kg

$$TIAC_{human} = TIAC_{mouse} \times \frac{m_{mouse}}{m_{human}},$$

by the ratio in organ weights of mouse and human, for example, for pancreas: m_{mouse} = 0.305 g and m_{human} = 94.3 g.

The extrapolated $TIAC_{human}$, multiplied by the reference man organ weight, was used as input to the dosimetry software OLINDA/EXM (*27*). Absorbed doses to the organs were derived for the reference male phantom. Fifty percent of the activity was considered to be distributed in the whole body (remainder), and the dynamic bladder model was used to derive the urinary bladder dose with 5 voids per day.

Statistics

Least-square fits with exponential curves were performed with Prism software (version 5.01; GraphPad Software). Decisions on the number of exponentials and plateau values were based on the Aikake information criterion, thereby balancing better fit correlation and degrees of freedom for the fit. A correlation coefficient $R^2 > 0.7$ was used as the lowest allowable goodness-of-fit criterion. Time–activity curves below this criterion were piecewise integrated by the trapezoidal method.

RESULTS

Biodistribution of ^{68}Ga-NeoBOMB1

The results of the biodistribution studies with approximately 13 MBq/250 pmol ^{68}Ga-NeoBOMB1 are presented in Figure 2. The highest tumor uptake of 12.4 ± 2.3 %ID/g of tissue was measured at 120 min after injection (Fig. 2A). At that time point, uptake in the pancreas was 22.7 ± 3.3 %ID/g of tissue. As a consequence of renal and hepatobiliary excretion, uptake values in the kidney and liver were 5.7 ± 2.4 and 8.3 ± 1.8 %ID/g of tissue, respectively. When receptors were blocked by coinjection with an excess of unlabeled NeoBOMB1, uptake in GRPR-expressing tissues, such

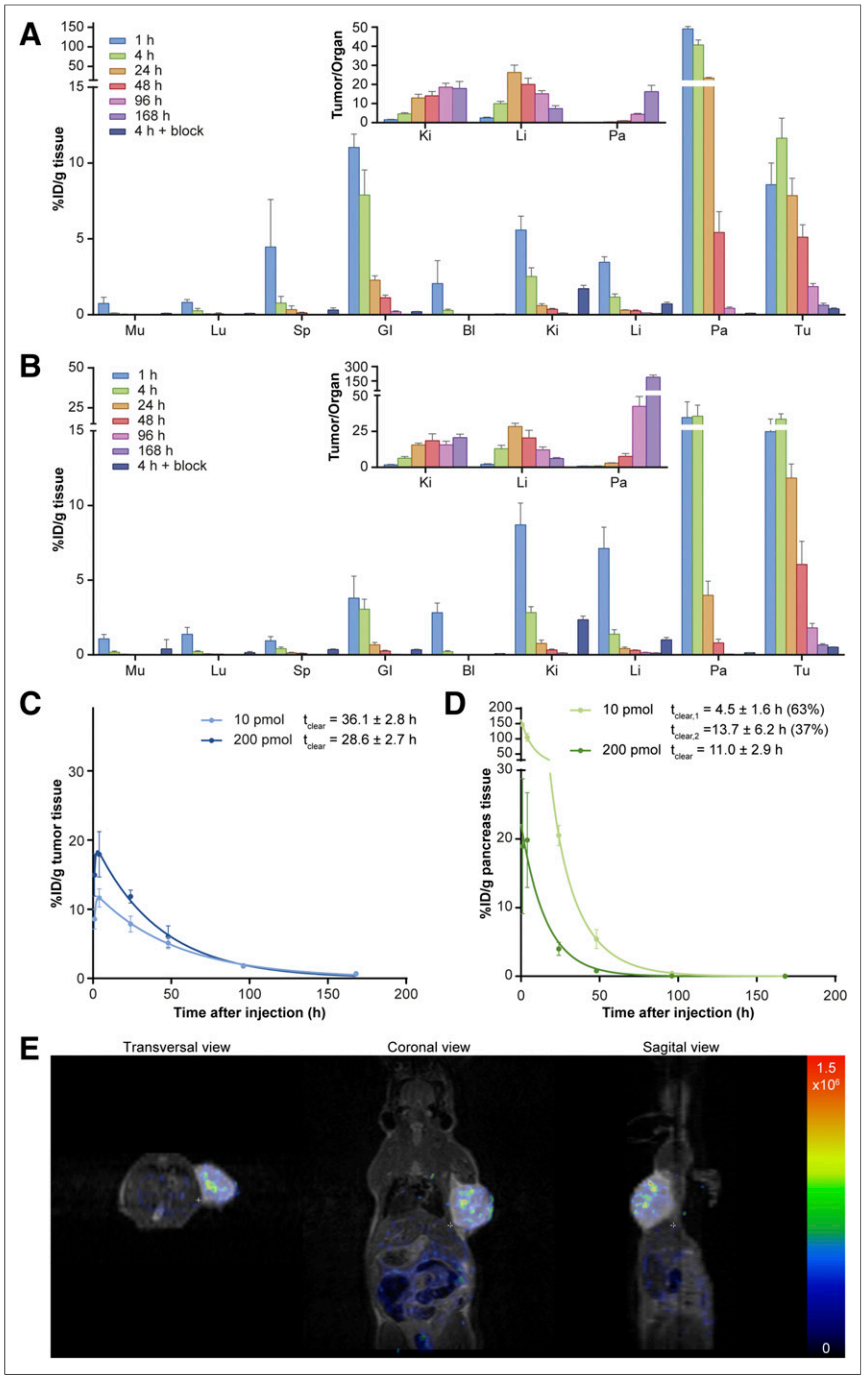

FIGURE 3. ^{177}Lu-NeoBOMB1 biodistribution and imaging. (A and B) Biodistribution of 200 and 10 pmol ^{177}Lu-NeoBOMB1 in PC-3–xenografted animals, respectively. Tumor-to-organ ratios are displayed in upper bar graph. (C) Pharmacokinetic modeling of ^{177}Lu-NeoBOMB1 tumor uptake. (D) Pharmacokinetic modeling of ^{177}Lu-NeoBOMB1 pancreas uptake. (E) SPECT/MR images 240 min after injection of 20 MBq/200 pmol ^{177}Lu-NeoBOMB1. Tumor is located on right shoulder. Bl = blood; Gl = gastrointestinal tract; Ki = kidney; Li = liver; Lu = lungs; Mu = muscle; Pa = pancreas; Sp = spleen; Tu = PC-3 tumor.

as tumor and pancreas, decreased to 1.0 ± 0.1 and 0.7 ± 0.1 %ID/g of tissue, respectively. Pharmacokinetic calculations resulted in a tumor clearance half-life of 6.9 ± 2.8 h and a pancreas clearance half-life of 12.9 ± 4.0 h (Figs. 2B and 2C). Clearance from blood proceeded according to a biphasic pattern: 66% ± 9%, with a half-life of 8 ± 5 min, and 34%, with a half-life of 50 ± 15 min.

PET/CT scans of animals injected with 11.5 MBq/230 pmol resulted in good visualization of the tumor tissue. As expected, uptake was also seen in the abdominal area as a consequence of uptake in the gastrointestinal tract or pancreas. Images are presented in Figure 2D.

Biodistribution of ^{177}Lu-NeoBOMB1

Injection of 1 MBq/10 pmol or 1 MBq/200 pmol ^{177}Lu-NeoBOMB1 in PC-3–xenografted mice resulted in a higher tumor uptake with 200 pmol ^{177}Lu-NeoBOMB1 than that obtained after injection of 10 pmol ^{177}Lu-NeoBOMB1 (17.9 ± 3.3 vs. 11.6 ± 1.3 %ID/g tissue 240 min after injection). Figure 3 shows the results of the ^{177}Lu-NeoBOMB1 biodistribution studies with 200 pmol (Fig. 3A) and with 10 pmol (Fig. 3B). Next to the tumor, high uptake was seen in the pancreas. However, in contrast to the tumor uptake, pancreas uptake was lower after injection of 200 pmol ^{177}Lu-NeoBOMB1 (19.8 ± 6.9 %ID/g tissue 240 min after injection) than injection of 10 pmol ^{77}Lu-NeoBOMB1 (105 ± 13 %ID/g 240 min after injection), resulting in a significant increase of the tumor-to-pancreas ratio with the higher peptide amount. Apart from the tumor and pancreas, the difference in peptide amount injected did not affect uptake in other non–GRPR-expressing organs (e.g., kidney uptake was 2.8 ± 0.4 vs. 2.5 ± 0.6 %ID/g tissue 240 min after injection of 200 and 10 pmol ^{177}Lu-NeoBOMB1, respectively). Uptake in tumor and pancreas was receptor-specific, because coinjection with an excess of unlabeled NeoBOMB1 resulted in a significant decrease of both tumor uptake (0.50 ± 0.02 and 0.39 ± 0.06 %ID/g of tissue using 200 and 10 pmol ^{177}Lu-NeoBOMB1, respectively) and pancreas uptake (0.13 ± 0.01 and 0.10 ± 0.01 %ID/g of tissue using 200 and 10 pmol ^{177}Lu-NeoBOMB1, respectively), independent of the peptide amount used.

Although initial radioactivity uptake in the pancreas was high, pancreas uptake decreased relatively rapidly, whereas tumor radioactivity was retained longer. The pharmacokinetic calculations resulted in a tumor clearance half-life of 28.6 ± 2.7 h and in a pancreas clearance half-life of 11.0 ± 2.9 h when animals were injected with 200 pmol ^{177}Lu-NeoBOMB1 (Figs. 3C and 3D). The tumor clearance half-life was 36.1 ± 2.8 h after injection of 10 pmol of the radiotracer. The clearance from the pancreas showed a biexponential pattern after injection of 10 pmol ^{177}Lu-NeoBOMB1: 63%, with a half-life of 4.5 ± 1.6 h, and 37%, with a half-life of 13.7 ± 6.2 h. After injection of 200 pmol ^{177}Lu-NeoBOMB1, only a single-exponential

TABLE 1
Absorbed Dose per Administered Activity (mGy/MBq) in 340 ± 100 mm^3 PC-3 Tumor Xenografts and Organs for ^{177}Lu-NeoBOMB1

Organ	10 pmol	200 pmol	*D*(*tumor*)/*D*(*organ*) 10 pmol	*D*(*tumor*)/*D*(*organ*) 200 pmol
Tumor	435	570	—	—
Kidneys	58	57	7.5	10
Pancreas	1393	265	0.31	2.15

curve could be fitted. Clearance from blood proceeded according to a single-phase pattern, with a half-life of 63 ± 32 min after injection of 10 pmol ^{177}Lu-NeoBOMB1 and 48 ± 12 min after injection of 200 pmol of the radiotracer.

SPECT/MR images acquired 240 min after injection of approximately 20 MBq/200 pmol of ^{177}Lu-NeoBOMB1 resulted in good visualization of the tumor (Fig. 3E). In line with the results of the biodistribution study, minimal uptake was observed in the gastrointestinal tract.

Dosimetry

Dosimetry calculations resulted in a higher tumor dose (581 vs. 435 mGy/MBq) and a lower dose to the pancreas (265 vs. 1,393 mGy/MBq) after injection of 200 pmol ^{177}Lu-NeoBOMB1 versus 10 pmol ^{177}Lu-NeoBOMB1 (Table 1). When animal data were used to predict human dosimetry according to method 2 (ratio of organ weights), we found a kidney, pancreas, and liver exposure of 0.10, 0.65, and 0.06 mGy/MBq, respectively (Table 2). Method 1 (ratio of body weights) yielded lower absorbed dose estimates.

DISCUSSION

Because overexpression of the GRPR is reported in various cancer types, targeting this receptor with radiolabeled peptide analogs for imaging and therapy might have a significant impact on patient care. In this study, we explored the use of a novel radiolabeled GRPR antagonist, NeoBOMB1, for tumor targeting by performing imaging and biodistribution studies in a prostate cancer mouse model. NeoBOMB1 is linked to a DOTA chelator and can be labeled with different radionuclides, enabling the theranostic use of the peptide analog. We evaluated the biodistribution of both ^{68}Ga-NeoBOMB1, for imaging purposes, and ^{177}Lu-NeoBOMB1, for therapy purposes, in a mouse model to generate information for theranostic use of the radiotracer.

Biodistribution studies with ^{68}Ga-NeoBOMB1 resulted in a high tumor uptake, leading to clear visualization of the tumor on PET/CT scans. Furthermore, relatively high uptake of ^{68}Ga-NeoBOMB1 was observed in the GRPR-expressing pancreas, resulting in a tumor-to-pancreas ratio of 0.6 (60 min after injection). Clearance half-lives demonstrated a lower clearance half-life for the tumor (6.9 ± 2.8 h) than the pancreas (12.9 ± 4.0 h). Presumably, this is a consequence of the limited time points studied in the ^{68}Ga-NeoBOMB1 biodistribution studies. Furthermore, tumor uptake was slower than pancreas uptake. Because of the short half-life of ^{68}Ga in combination with the slower tumor kinetics, biodistribution studies could not be performed at later time points. Nevertheless, the presented data indicate that NeoBOMB1 has excellent pharmacokinetic properties for imaging.

In the ^{177}Lu-NeoBOMB1 biodistribution studies, we compared organ and tumor uptake of 2 different peptide amounts, 1 MBq/10 pmol and 1 MBq/200 pmol. Injection of 1 MBq/200 pmol ^{177}Lu-NeoBOMB1 resulted in a higher tumor uptake and a lower pancreatic uptake than the uptake observed after administration of 1 MBq/10 pmol ^{177}Lu-NeoBOMB1, resulting in a favorable tumor-to-pancreas ratio (0.9 vs. 0.11, based on radioactivity uptake 4

TABLE 2
Extrapolated Human Dosimetry (mGy/MBq) for ^{177}Lu-NeoBOMB1

Organ	10 pmol Method 1	10 pmol Method 2	200 pmol Method 1	200 pmol Method 2
Lower large intestine wall	0.18	0.32	0.17	0.18
Small intestine	0.17	0.19	0.15	0.16
Stomach wall	0.16	0.19	0.15	0.17
Upper large intestine wall	0.23	0.34	0.17	0.21
Heart wall	0.02	0.02	0.01	0.01
Kidneys	0.03	0.09	0.03	0.10
Liver	0.15	0.03	0.03	0.06
Lungs	0.02	0.01	0.01	0.01
Muscle	0.01	0.01	0.01	0.01
Pancreas	0.54	3.37	0.11	0.65
Red marrow	0.11	0.10	0.11	0.11
Osteogenic cells	0.44	0.42	0.45	0.44
Spleen	0.02	0.03	0.01	0.02
Urinary bladder wall	0.75	0.74	0.75	0.75
Total body	0.15	0.14	0.15	0.15

TABLE 3
Comparison Between Extrapolated and Determined Absorbed Doses per Injected Activity for ^{177}Lu-DOTA-Tyr^3-Octreotate

Organ	Method 1*	Method 2*	^{177}Lu-DOTA-Tyr^3-octreotate in patients†
Kidneys	0.06	0.16	0.62 (0.49–0.75)
Liver	0.01	0.01	0.29 (0.21–0.49)
Red marrow	0.11	0.11	0.016 (0.012–0.022)
Spleen	0.01	0.02	0.68 (0.51–0.92)
Total body	0.14	0.14	

*Data based on published data by Bison et al. (*32*).
†Data published by Sandström et al. (*33*).

h after injection) with the high peptide amount used. In contrast to the GRPR-positive pancreas, the uptake in other organs was not influenced by the injected peptide amount. The observed peptide amount–dependent uptake in the pancreas is likely due to partial receptor saturation of the pancreas when 200 pmol of the radiotracer is administered. Our results are in line with previous observations (*8,28*) for the GRPR agonist AMBA and emphasize the need for careful optimization of protocols for nuclear imaging and therapy.

Furthermore, dosimetry calculations resulted in a 1.3-times-higher tumor dose and a 5-times-lower pancreas dose with 200 pmol ^{177}Lu-NeoBOMB1 than 10 pmol ^{177}Lu-NeoBOMB1. When dosimetry data are compared with other radiolabeled GRPR antagonists, such as ^{177}Lu-JMV4168 (*29*), estimated absorbed radiation doses to the tumor were higher for ^{177}Lu-NeoBOMB1 (29 Gy/50 MBq vs. 11 Gy/50 MBq) even when ^{177}Lu-JMV4168 was stabilized by coinjection of an enzyme inhibitor (29 Gy/50 MBq vs. 20 Gy/MBq). When we compared the dose to the kidneys and pancreas of the radiotracers, we found a more favorable tumor-to-kidney ratio for ^{177}Lu-NeoBOMB1 (10 vs. 1.5) and a similar tumor-to-pancreas ratio (2.2 vs. 2.5).

As expected, when the biodistribution of the ^{68}Ga-NeoBOMB1 or ^{177}Lu-NeoBOMB1 was compared with the uptake of radiolabeled GRPR agonists, for example, ^{99m}Tc-demobesin4 or ^{177}Lu-AMBA, a lower uptake was observed in GRPR-expressing organs, namely the pancreas and the gastrointestinal tract (*8,13*).

Comparing uptake and dosimetry of radiolabeled NeoBOMB1 with other radiolabeled GRPR antagonists mentioned in the literature is difficult because of the differences between experimental conditions, such as the peptide amount used and the radionuclide bound to the peptide. However, we can report that the in vivo tumor-to-pancreas ratios in mouse models are more favorable for ^{68}Ga-NeoBOMB1 (0.6) than other GRPR antagonists such as ^{67}Ga-SB3 (0.2) reported by Maina et al. (*16*) and ^{99m}Tc-Demobesin 1 (0.2) reported by Cescato et al. (numbers are based on biodistribution results 60 min after injection of the radiotracers) (*13*). However, lower peptide amounts were used in these studies, which could lead to less favorable results as demonstrated in the ^{177}Lu-NeoBOMB1 biodistribution studies. Nevertheless, the mentioned radiotracers have successfully been used in clinical trials for the visualization of both breast and newly diagnosed prostate cancer lesions, emphasizing the potential of ^{68}Ga-NeoBOMB1 for tumor visualization in humans.

Comparing extrapolated human dosimetry data of ^{177}Lu-NeoBOMB1 with extrapolated dosimetry data of ^{177}Lu-DOTA-Tyr^3-octreotate, which is currently successfully used for treatment of patients with neuroendocrine tumors, we found similar values (Table 3). This was expected because excretion patterns of the 2 radiotracers are comparable. Although the extrapolated dosimetry data of ^{177}Lu-DOTA-Tyr^3-octreotate do not completely fit the dosimetry values obtained from patient studies (Table 3), based on the extrapolated data of ^{177}Lu-NeoBOMB1, we expect similar values.

Concerning imaging, patient studies by Maina et al. (*16*) in which prostate cancer lesions were successfully visualized using a GRPR radioligand showed a biodistribution pattern in physiologic organs similar to what was found in mice. However, this was a pilot study in a limited number of patients, and more clinical studies are needed.

Promising prostate-specific membrane antigen (PSMA)–targeting ligands are currently also under investigation for the same purpose. In a recent study, Minamimoto et al. (*30*) compared PSMA and GRPR-targeted imaging in prostate cancer and found no significant differences. Furthermore, Perera et al. (*31*) reported on a relatively low sensitivity of PSMA-targeted imaging in patients with low prostate-specific antigen levels and patients with primary disease (40% and 50%, respectively). Especially in these patient groups, the application of GRPR radioligands may be of benefit.

CONCLUSION

On the basis of the presented data, both ^{68}Ga-NeoBOMB1 and ^{177}Lu-NeoBOMB1 have excellent tumor uptake and favorable pharmacokinetics for theranostic use. Clinical studies using these radiotracers in GRPR-expressing cancer, for example, prostate cancer and breast cancer, have yet to be performed, but expectations are high.

DISCLOSURE

This study was partly funded by Advanced Accelerator Applications. No other potential conflict of interest relevant to this article was reported.

REFERENCES

1. Guo M, Qu X, Qin XQ. Bombesin-like peptides and their receptors: recent findings in pharmacology and physiology. *Curr Opin Endocrinol Diabetes Obes.* 2015;22:3–8.

2. Gonzalez N, Moody TW, Igarashi H, Ito T, Jensen RT. Bombesin-related peptides and their receptors: recent advances in their role in physiology and disease states. *Curr Opin Endocrinol Diabetes Obes.* 2008;15:58–64.
3. Gugger M, Reubi JC. Gastrin-releasing peptide receptors in non-neoplastic and neoplastic human breast. *Am J Pathol.* 1999;155:2067–2076.
4. Markwalder R, Reubi JC. Gastrin-releasing peptide receptors in the human prostate: relation to neoplastic transformation. *Cancer Res.* 1999;59:1152–1159.
5. Brabander T, Kwekkeboom DJ, Feelders RA, Brouwers AH, Teunissen JJ. Nuclear medicine imaging of neuroendocrine tumors. *Front Horm Res.* 2015; 44:73–87.
6. Kwekkeboom DJ, Krenning EP. Peptide receptor radionuclide therapy in the treatment of neuroendocrine tumors. *Hematol Oncol Clin North Am.* 2016;30: 179–191.
7. Yu Z, Ananias HJ, Carlucci G, et al. An update of radiolabeled bombesin analogs for gastrin-releasing peptide receptor targeting. *Curr Pharm Des.* 2013;19:3329–3341.
8. Lantry LE, Cappelletti E, Maddalena ME, et al. ^{177}Lu-AMBA: synthesis and characterization of a selective ^{177}Lu-labeled GRP-R agonist for systemic radiotherapy of prostate cancer. *J Nucl Med.* 2006;47:1144–1152.
9. Schroeder RP, Muller C, Reneman S, et al. A standardised study to compare prostate cancer targeting efficacy of five radiolabelled bombesin analogues. *Eur J Nucl Med Mol Imaging.* 2010;37:1386–1396.
10. Nock B, Nikolopoulou A, Chiotellis E, et al. [^{99m}Tc]demobesin 1, a novel potent bombesin analogue for grp receptor-targeted tumour imaging. *Eur J Nucl Med Mol Imaging.* 2003;30:247–258.
11. Mather SJ, Nock BA, Maina T, et al. GRP receptor imaging of prostate cancer using [^{99m}Tc]demobesin 4: a first-in-man study. *Mol Imaging Biol.* 2014;16: 888–895.
12. Mansi R, Wang X, Forrer F, et al. Development of a potent DOTA-conjugated bombesin antagonist for targeting GRPr-positive tumours. *Eur J Nucl Med Mol Imaging.* 2011;38:97–107.
13. Cescato R, Maina T, Nock B, et al. Bombesin receptor antagonists may be preferable to agonists for tumor targeting. *J Nucl Med.* 2008;49:318–326.
14. Ginj M, Zhang H, Waser B, et al. Radiolabeled somatostatin receptor antagonists are preferable to agonists for in vivo peptide receptor targeting of tumors. *Proc Natl Acad Sci USA.* 2006;103:16436–16441.
15. Bodei L, Ferrari M, Nunn AD, et al. ^{177}Lu-AMBA bombesin analogue in hormone refractory prostate cancer patients: a phase I escalation study with single-cycle administrations [abstract]. *Eur J Nucl Med Mol Imaging.* 2007;34: S221.
16. Maina T, Bergsma H, Kulkarni HR, et al. Preclinical and first clinical experience with the gastrin-releasing peptide receptor-antagonist [Ga]SB3 and PET/CT. *Eur J Nucl Med Mol Imaging.* 2016;43:964–973.
17. Heimbrook DC, Saari WS, Balishin NL, et al. Gastrin releasing peptide antagonists with improved potency and stability. *J Med Chem.* 1991;34: 2102–2107.
18. Nock B, Kaloudi A, Lymperis E, et al. [^{68}Ga]NeoBomb1, a new potent GRPR-antagonist for PET imaging: preclinical and first clinical evaluation in prostate cancer [abstract]. *J Nucl Med.* 2016;57(suppl 2):583.
19. Dalm S, Bakker I, de Blois E, et al. ^{68}Ga/^{177}Lu-NeoBOMB1, a novel radiolabeled GRPR antagonist for theranostic use [abstract]. *J Nucl Med.* 2016; 57(suppl 2):331.
20. Maina-Nock T, Nock BA, de Jong M, inventors; Biosynthema Inc., assignee. Grpr-antagonists for detection, diagnosis and treatment of grpr-positive cancer. Google patents. April 3, 2014.
21. Breeman WA, de Zanger RM, Chan HS, de Blois E. Alternative method to determine specific activity of ^{177}Lu by HPLC. *Curr Radiopharm.* 2015;8: 119–122.
22. Castaldi E, Muzio V, D'Angeli L, Fugazza L. ^{68}GaDOTATATE lyophilized ready to use kit for PET imaging in pancreatic cancer murine model [abstract]. *J Nucl Med.* 2014;55(suppl 1):1926.
23. Keenan MA, Stabin MG, Segars WP, Fernald MJ. RADAR realistic animal model series for dose assessment. *J Nucl Med.* 2010;51:471–476.
24. Bolch WE, Eckerman KF, Sgouros G, Thomas SR. MIRD pamphlet no. 21: a generalized schema for radiopharmaceutical dosimetry—standardization of nomenclature. *J Nucl Med.* 2009;50:477–484.
25. Stabin MG, Konijnenberg MW. Re-evaluation of absorbed fractions for photons and electrons in spheres of various sizes. *J Nucl Med.* 2000;41: 149–160.
26. Stabin MG. *Fundamentals of Nuclear Medicine Dosimetry.* 1st ed. New York, NY: Springer-Verlag; 2008.
27. Stabin MG, Sparks RB, Crowe E. OLINDA/EXM: the second-generation personal computer software for internal dose assessment in nuclear medicine. *J Nucl Med.* 2005;46:1023–1027.
28. De Blois E, Schroeder RJ, De Ridder CA, Van Weerden WM, Breeman WP, De Jong M. Improving radiopeptide pharmacokinetics by adjusting experimental conditions for bombesin receptor-mediated imaging of prostate cancer. *Q J Nucl Med Mol Imaging.* June 9, 2013 [Epub ahead of print].
29. Chatalic KL, Konijnenberg M, Nonnekens J, et al. In vivo stabilization of a gastrin-releasing peptide receptor antagonist enhances PET imaging and radionuclide therapy of prostate cancer in preclinical studies. *Theranostics.* 2016;6: 104–117.
30. Minamimoto R, Hancock S, Schneider B, et al. Pilot comparison of ^{68}Ga-RM2 PET and ^{68}Ga-PSMA-11 PET in patients with biochemically recurrent prostate cancer. *J Nucl Med.* 2016;57:557–562.
31. Perera M, Papa N, Christidis D, et al. Sensitivity, specificity, and predictors of positive ^{68}Ga-prostate-specific membrane antigen positron emission tomography in advanced prostate cancer: a systematic review and meta-analysis. *Eur Urol.* June 27, 2016 [Epub ahead of print].
32. Bison SM, Konijneberg MW, Koelewijn SJ, Melis ML, de Jong M. Influence of specific activity on tumour dosimetry and response to therapy in a nude mouse small cell lung cancer model. *Eur J Nucl Med Mol Imaging.* 2014;41(suppl 2): S280–S281.
33. Sandström M, Garske-Roman U, Granberg D, et al. Individualized dosimetry of kidney and bone marrow in patients undergoing ^{177}Lu-DOTA-octreotate treatment. *J Nucl Med.* 2013;54:33–41.